How to cite: *Angew. Chem. Int. Ed.* **2022,** *61,* e202210242
International Edition: doi.org/10.1002/anie.202210242
German Edition: doi.org/10.1002/ange.202210242

Graphdiyne Hot Paper

A Deprotection-free Method for High-yield Synthesis of Graphdiyne Powder with In Situ Formed CuO Nanoparticles

Jian Li, Xu Han, Dongmei Wang, Lei Zhu, Minh-Huong Ha-Thi, Thomas Pino, Jordi Arbiol, Li-Zhu Wu, and Mohamed Nawfal Ghazzal**

Abstract: With a direct band gap, superior charge carrier mobility, and uniformly distributed pores, graphdiyne (GDY) has stimulated tremendous interest from the scientific community. However, its broad application is greatly limited by the complicated multistep synthesis process including complex deprotection of hexakis-[(trimethylsilyl)ethynyl]benzene (HEB-TMS) and peeling of GDY from the substrates. Here, we describe a deprotection-free strategy to prepare GDY powder by directly using HEB-TMS as the monomer. When CuCl was used as the catalysts in DMF solvent, the yield of GDY powder reached ≈100 %. More interestingly, uniformly dispersed CuO nanoparticles with an average diameter of ≈2.9 nm were in situ formed on GDY after the reaction. The prepared CuO/GDY was demonstrated an excellent co-catalyst for photocatalytic hydrogen evolution, comparable to the state-of-art Pt co-catalyst. The deprotection-free approach will widen the use of GDY and facilitate its scaling up to industrial level.

Introduction

Graphdiyne (GDY), consisting of sp- and sp^2-hybridized carbon atoms, emerges as a rising-star two-dimensional carbon material[1] and has triggered huge research interest from theoretical investigations[2] and practical applications.[3] The large π-conjugated network, formed by benzene rings and acetylenic linkages, endows GDY with uniformly distributed pores, a direct band gap, large surface area, and high intrinsic charge carrier mobility.[4] These unique attributes have shown great potential in diverse applications such as catalysis,[5,6] Li-ion battery,[7] environmental remediation,[8] and solar cells.[9] Despite tremendous progress in the synthesis of GDY for different applications,[10,11] there is still a need to ease the synthesis process and realize mass production for broader potential applications.

The first experimental synthesis of GDY film was achieved on copper foil via Glaser coupling reactions,[12] where copper foil serves as both the catalyst and the substrate. Since then, tremendous efforts have been dedicated to advancing the experimental synthesis of GDY. A series of original methods have been developed, such as a Cu envelope strategy,[13] interfacial coupling method,[14] van der Waals epitaxial growth strategy,[15] and explosion method,[16] which enable the controllable preparation of GDY in terms of thickness, dimension, and morphology. However, the currently reported synthesis of GDY requires a preliminary deprotection of hexakis-[(trimethylsilyl)ethynyl]benzene (HEB-TMS) under an inert atmosphere due to the severe sensitivity of HEB monomer to air. Such a process is complicated and costly in actual production and the peeling of GDY from the substrates reduces the yield of independent GDY. Recently, a triazine-based graphdiyne film was prepared directly from 2,4,6-tris(4-[(trimeth-

[*] Dr. J. Li, Prof. Dr. M. Nawfal Ghazzal
Université Paris-Saclay, UMR 8000 CNRS, Institut de Chimie Physique
91405 Orsay (France)
E-mail: mohamed-nawfal.ghazzal@universite-paris-saclay.fr
X. Han, Prof. Dr. J. Arbiol
Catalan Institute of Nanoscience and Nanotechnology (ICN2), CSIC and BIST, Campus UAB
Bellaterra, 08193 Barcelona, Catalonia (Spain)
D. Wang
CAS Key Laboratory for Biomedical Effects of Nanomaterials and Nano safety, Institute of High Energy Physics, Chinese Academy of Sciences
Beijing 100049 (China)
L. Zhu, Prof. Dr. L.-Z. Wu
Key Laboratory of Photochemical Conversion and Optoelectronic Materials, Technical Institute of Physics and Chemistry & University of Chinese Academy of Sciences, Chinese Academy of Sciences
Beijing 100190 (P. R. China)
E-mail: lzwu@mail.ipc.ac.cn
Dr. M.-H. Ha-Thi, Dr. T. Pino
Université Paris-Saclay, CNRS, Institut des Sciences Moléculaires d'Orsay
91405 Orsay (France)
Prof. Dr. J. Arbiol
ICREA
Pg. Lluís Companys 23, 08010 Barcelona, Catalonia (Spain)

ylsilyl)ethynyl]phenyl)-1,3,5-triazine (TMS-Tz) monomers over a commercial copper foil surface.[17] However, the synthesis of GDY powder by directly using HEB-TMS as a monomer is still in fancy. Therefore, developing a deprotection-free synthesis method to achieve the mass production of GDY with a high yield is imperative for its broad application.

Furthermore, although Cu substrate or salts are used as catalysts for the synthesis of GDY, almost no attention has been paid to the final states of Cu species. The reported wet-chemistry approaches focus on the removal of the catalyst residue rather than considering the advantages of the Cu species. Actually, Cu is one of the most promising transition metal catalysts,[18] and the use of Cu to grow GDY provides an in situ formed tight junction at the interface, facilitating charge separation/transfer and surface reaction kinetics.[19] Full utilization of the Cu species in the synthesis of GDY will definitely exhibit extraordinary catalytic activity.

With this in mind, we initiated an efficient and straightforward deprotection-free method that allows the direct coupling reactions of HEB-TMS based on variable copper-based catalysts and solvents at 60 $_{\circ}$C in air. When CuCl and N,N-Dimethylformamide (DMF) were used as the catalyst and solvent, respectively, the yield of GDY powder was as high as $\approx$100 %. Most interestingly, uniform CuO nanoparticles with an average diameter of $\approx$2.9 nm were in situ loaded on the surface of GDY after the reaction. Pure GDY powder could be further obtained after using 0.5 M HCl to remove CuO. To demonstrate the potential of the prepared CuO/GDY, TiO_2 as a reference semiconductor was hybridized with CuO/GDY for photocatalytic hydrogen generation. Owing to the solid junction between GDY and CuO, the CuO/GDY as cocatalysts promoted photocatalytic activity remarkably with an H_2 evolution rate of 18 mmol h^{-1} g^{-1}, comparable to that of 0.5 % Pt loaded TiO_2. This work demonstrates a facile deprotection-free approach for large-scale synthesis of GDY with 100 % yield and provides an alternative prospect for applying GDY in diverse applications.

Results and Discussion

It has been demonstrated that alkynylsilanes can dimerize with Cu^I salt as catalysts in polar solvents such as N,N-dimethyformamide (DMF), and dimethyl sulfoxide (DMSO) to produce 1,3-conjugated diynes.[20] Inspired by these works, we first examined the direct coupling reaction of HEB-TMS in DMF by using CuCl as the catalysts. In brief, HEB-TMS and CuCl with the molecular proportion of 1:1 were added to DMF and placed in a closed reaction tube. After reaction at 60 °C for 24 h under aerobic conditions, black precipitate appeared on the bottom of the tube (Figure 1a). The generated solid was recovered by centrifugation and washed consecutively by DMF, THF, and water (Figure S1).

Optimal conditions of the deprotection-free synthesis of GDY were further investigated over various solvents and different Cu-based catalysts. The yields of GDY after the coupling reactions are strongly sensitive to the nature of the solvent, as summarized in Table S1 and Figure 1b. DMF was found to be the best solvent in promoting the coupling reaction, reaching a yield up to $\approx$100 %. In sharp contrast, few amounts of the desired product were obtained in a protic or less polar solvent, such as EtOH, CH_3CN, pyridine, and diethyl ether. It is worth noting that no trace of GDY was obtained in aprotic and polar DMSO, which is probably due to the poor solubility of the HEB-TMS monomer. Thus, the use of DMF is essential to promote the direct coupling reaction of the HEB-TMS monomer. The effect of the copper oxidation states on GDY yield was also systematically studied (Figure 1c). All the copper (I) salts, including CuCl, CuBr, and CuI, can efficiently promote the reaction, reaching almost $\approx$100 % yield of GDY. Conversely, Cu^{II} species, such as $CuCl_2$, CuO, and $Cu(OH)_2$ were inactive for the coupling reaction. Cu_2O and CuCN, which have been reported as partially active for the alkynylsilanes dimerization, showed no activity for the GDY polymerization.

Given the above results, CuCl and DMF were selected as the catalyst and solvent, respectively, for the direct and deprotection-free coupling reaction of HEB-TMS, because of the high yield and easy handling in air. The effect of the stoichiometric ratio between CuCl and HEB-TMS on the yield was further investigated. When decreasing the stoichiometric ratio between CuCl and HEB-TMS to 1:2, the yield of GDY decreased to $\approx$55 %. In contrast, when increasing the stoichiometric ratio between CuCl and HEB-TMS to 2:1 even to 4:1, the yield of GDY kept $\approx$100 %. Therefore, the stoichiometric ratio of 1:1 between HEB-TMS and CuCl is the optimal ratio, because it can achieve the complete coupling reaction of HEB-TMS with least amount of CuCl. To gain insight into the mechanism, the reaction was carried out using CuCl in DMF under an Ar atmosphere. The yield of GDY powder decreased remarkably to $\approx$40 %, indicating the crucial role of oxygen in the process. A possible reaction mechanism was further proposed (Figure 1d). HEB-TMS first reacted with CuCl to form an intermediate, presumably organocopper (I) species,[20] which then underwent reductive elimination of Cu^0 during the formation of the butadiyne bridge. The produced Cu^0 will be further oxidized into Cu^I in the presence of air for the next catalytic cycle. Meanwhile, part of Cu^I was also oxidized to Cu^{II}. In this mechanism, trimethylsilyl chloride (TMS-Cl) was generated and then converted to TMS-OH and TMS-O-TMS, as confirmed by GC-MS (Figure S2).

UV/Vis absorption and Raman spectroscopy were used to study the chemical structure of the prepared powder. In comparison to HEB-TMS, the UV/Visible spectrum of the black powder showed a noticeable bathochromic shift. Such redshift represents the enlarged electron delocalization by the extended π-conjugated system,[21] confirming the successful formation of conjugated diacetylenic linkages (Figure 2a). The Raman spectrum showed four prominent bands, which are recognized as the fingerprint of graphdiyne (Figure 2b). The breathing vibration of sp^2 carbon domains of aromatic rings (D band) was confirmed by the presence

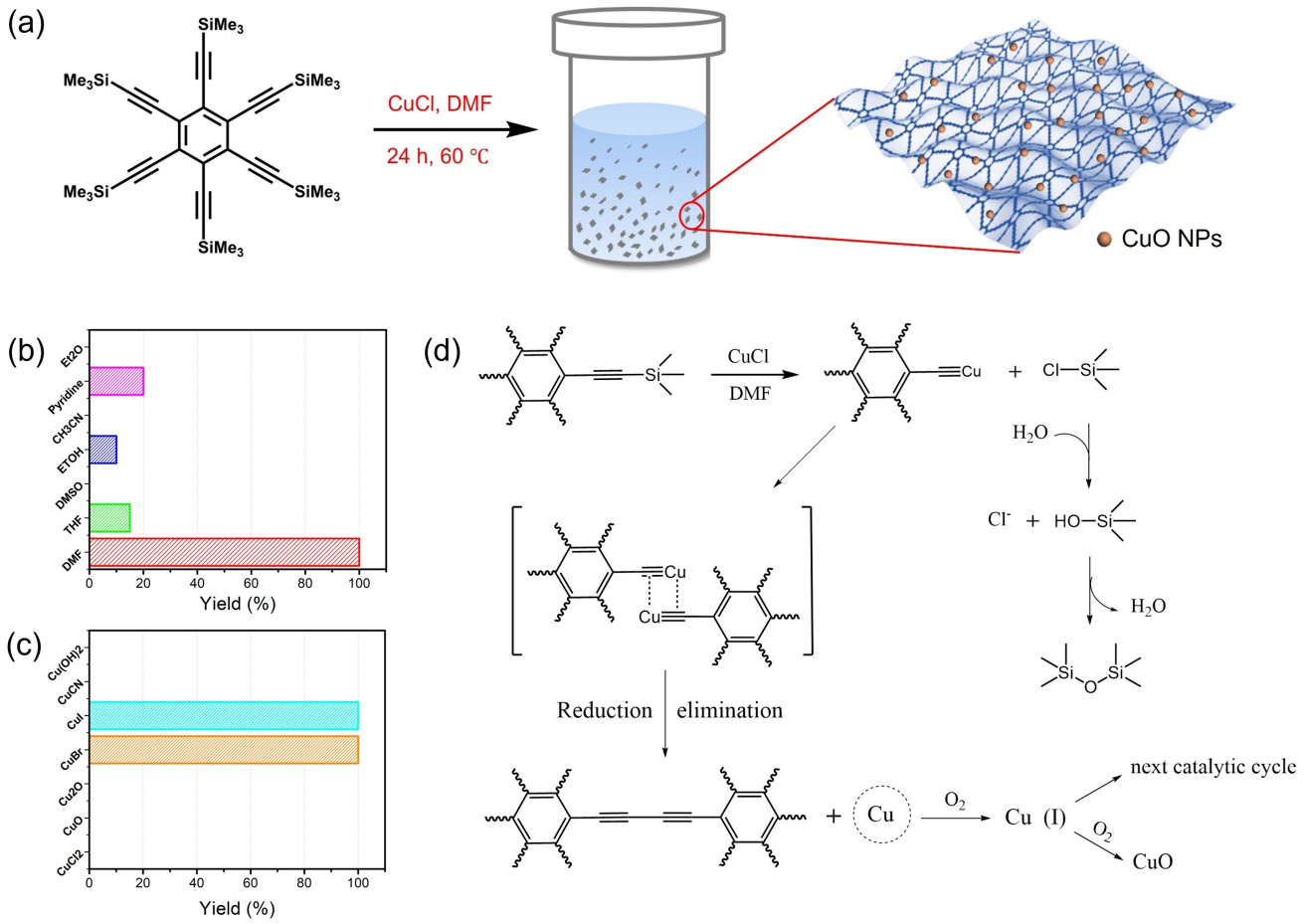

Figure 1. The direct coupling reaction of HEB-TMS and the proposed catalytic mechanism. a) Schematic diagram of direct synthesis of GDY with in situ formed CuO nanoparticles; b) HEB-TMS coupling reaction yield with CuCl in different solvents; c) HEB-TMS coupling reaction yield with various Cu salts in DMF solvent; d) the proposed possible catalytic mechanism of the reaction.

of a peak at 1387.8 cm^{-1}. The peak located at 1568.5 cm^{-1} is assigned to the first-order scattering of the E2 g mode for in-phase stretching vibration sp^2 carbon lattice (G band) in aromatic rings, and the peaks at 1924.1 and 2173.8 cm^{-1} are attributed to the vibration of the conjugated diyne linkage (–C≡C–C≡C–). X-ray photoelectron spectroscopy (XPS) and X-ray diffraction (XRD) were also performed to investigate the chemical composition, chemical state, and chemical bonds of the prepared GDY composites. The XPS general survey of the synthesized powder indicated mainly the presence of C, O, and Cu (Figure 2c). The High-resolution XPS spectrum of the Cu 2p exhibited two prominent peaks resolved at 933.6 (Cu $2p_{3/2}$) and 953.5 eV (Cu $2p_{1/2}$), accompanied by a noticeable satellite (Figure 2d), which is directly related to the characteristic signals of CuO.[22] Furthermore, two distinct peaks at 36.6° and 42.5° were observed in the XRD spectra of the prepared powder (Figure 2e). These two peaks correspond to the (111) and (200) crystalline planes of Cubic CuO, respectively (PDF: 78-0428). Inductively coupled plasma mass spectrometry (ICP-MS) was used to calculate the amount of the formed CuO. Based on the weight percent of element Cu (7.88 %), the corresponding weight percent of CuO was calculated to be ≈9.85 % (Figure S3).

The morphology and composition of the as-prepared powder were then characterized by scanning electron microscope (SEM) and transmission electron microscope (TEM). SEM images displayed the morphology of the sphere-shaped flakes (Figure S4). Electron energy loss spectroscopy (EELS) mapping of the selected region displayed a uniform distribution of Cu, O, and C elements, further suggesting the existence of Cu species in the composite (Figure 3a,b). The high-resolution TEM (HRTEM) micrograph revealed that the nanoparticles loaded on GDY exhibited narrower size distribution with an average diameter of around ≈2.9 nm (Figure 3c,d). The NPs exhibited a crystal phase, which can be assigned to the cubic CuO (space group = Fm3 m) with $a = b = c = 4.2450$ Å (Figure 3e,f). The lattice fringe distances were measured to be 0.245 nm, 0.217 nm, and 0.245 nm at 56.48° and 111.40°, corresponding to (1-1-1), (200), and (111) planes of cubic CuO (Figure 3g), in agreement with the theoretical simulation and XRD results (Table S2, Figure S5). All of the above results indicated the successful synthesis of GDY with in situ formed CuO nanoparticles (NPs).

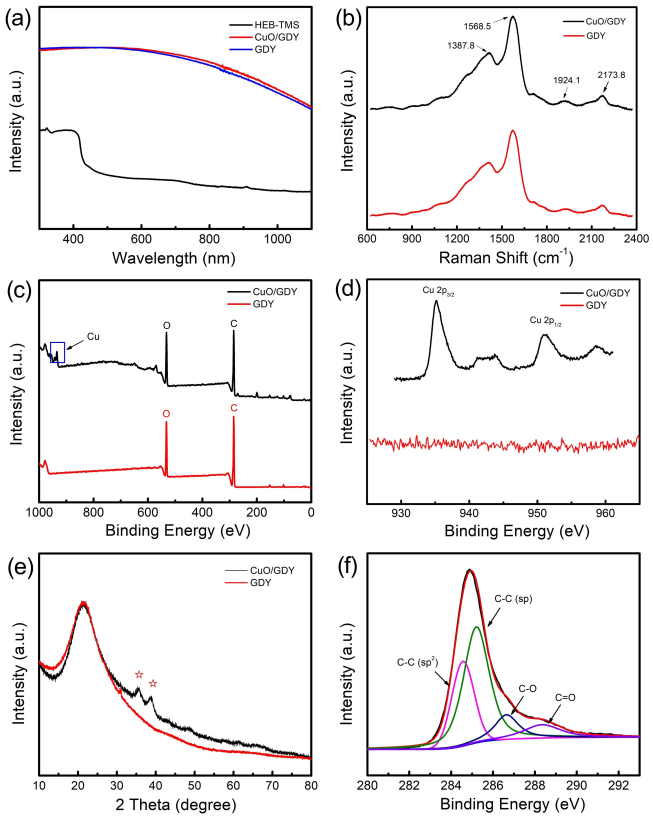

Figure 2. The characterization of the as-prepared CuO/GDY and GDY. a) UV/Vis spectra of monomer HEB-TMS, CuO/GDY, and pure GDY; b) Raman spectrum of CuO/GDY and pure GDY; c) XPS survey spectrum and d) high-resolution Cu 2p spectrum of CuO/GDY and pure GDY; e) XRD spectra of CuO/GDY and pure GDY; and f) high-resolution C 1s spectrum of pure GDY.

Pure GDY was further obtained by using hydrochloric acid to remove the CuO. In comparison with CuO/GDY, there was almost no difference in the UV/Vis and Raman spectra (Figure 2a,b), indicating that the chemical structure of GDY kept unchanged after acid treatment. The absence of Cu signals in XPS spectra and the disappearance of CuO peaks in the XRD spectra confirmed that the CuO NPs were removed entirely (Figure 2c–e). The broad diffraction peak located at around 22° is assigned to the (002) plane of graphite-type carbon, which reveals a distortion from the ordered arrangement of GDY along its stacking direction (Figure 2e). The peaks around ≈100 eV in XPS spectra belonged to organic Si, which possibly originate from the terminal unreacted TMS (Figure S6). The high-resolution XPS peak for C 1s peak was deconvoluted into four peaks, assigned to sp^2 (C=C) at 284.5 eV, sp (C≡C) at 285.2 eV, C=O at 288.5 eV, and C–O at 286.9 eV, respectively, which is in line with the GDY synthesized on Cu substrates (Figure 2f). The C=O species may originate from air of traces of impurities or oxygen defects in the GDY. The oxygen/carbon ratio in the pure GDY was determined as ≈1:3.3 by XPS (Table S3). The TEM images showed that GDY consisted of a few dispersed thin layers (Figure 3h), where the interlayer spacing was calculated to be 0.37 nm (Figure 3i), in agreement with the theoretical interlayer spacing of GDY (≈0.36 nm).[23]

To demonstrate the value of the prepared CuO/GDY as catalysts, TiO_2 as a representive semiconductor was coupled with CuO/GDY to test the photocatalytic activity towards H_2 evolution. The microstructure of the CuO/GDY/TiO_2 composite was characterized by TEM. As shown in Figure 4a, CuO NPs deposited on TiO_2 were clearly observed and EELS mapping of the selected region revealed the Ti, O, Cu, and C enriched areas of the sample (Figure 4b). The different distributions of C, Ti, and Cu confirmed that the sample consisted of three composite phases. HRTEM images provided further evidence of the close interface junction between TiO_2, GDY, and CuO, which was beneficial to the interfacial transfer of photogenerated charge (Figure 4c). The observed spots in the power spectrum (FFT) obtained in the HRTEM image correspond to the (1−12), (1−1−2), and (004) crystal planes of anatase TiO_2 (Figure 4d–f). XRD patterns, Raman, and XPS spectra were further performed to investigate the composition and chemical structure of CuO/GDY/TiO_2. XRD exhibited similar diffraction peaks for TiO_2 and hybrid CuO/GDY/TiO_2, regardless of the ratio (Figure S7). Due to their relatively small amount, no obvious diffraction patterns for GDY and CuO were observed. Raman spectra exhibited five bands at 144, 197, 397, 518, and 637 cm^{-1}, ascribed to the anatase TiO_2 phase (Figure S8). Two additional weak peaks at 1361 and 1596 cm^{-1}, observed for the CuO/GDY/TiO_2 nanocomposites, confirmed the presence of GDY. In fact, their intensity increases in proportion to the GDY content. However, the peak at 2172.1 cm^{-1}, representing the vibration of conjugated diyne linkers, was not observed because of the low content of GDY in the composites. Notably, compared to pristine TiO_2, the peaks around 144 cm^{-1} of CuO/GDY/TiO_2 shifted to a higher wavelength (Figure S8b), indicating the strong interaction between TiO_2 and GDY, which is in agreement with HRTEM observations. Compared to bare TiO_2 in the XPS spectra, additional Cu was detected for CuO/GDY/TiO_2 nanocomposites (Figure S9). The strong satellite peaks in the high-resolution XPS spectrum of the Cu 2p confirmed the existence of Cu^{2+}, as observed in the CuO/GDY sample (Figure S9b). UV/Vis diffuse reflectance spectra showed that the introduction of CuO/GDY had little effect on the absorption properties of TiO_2 samples (Figure S10).

The photocatalytic activity of the ternary CuO/GDY/TiO_2 nanocomposite was then evaluated for H_2 production under Xenon lamp illumination. In the absence of CuO/GDY, the pristine TiO_2 showed negligible photocatalytic activity. A remarkable increase in photocatalytic H_2 production was achieved when coupled with CuO/GDY (Figure 5a), indicating the key role of CuO/GDY as co-catalysts. The photocatalytic activity increased with the content of CuO/GDY and reached an optimal photoactivity for 5 % CuO/GDY/TiO_2. The total amount of H_2 generated by the 5 % CuO/GDY/TiO_2 was up to 1.08 mmol after 6 hours, which corresponds to 18 $mmol\,h^{-1}\,g^{-1}$ H_2 production rate (Figure 5b). A decreased performance was observed with further increase of the CuO/GDY content, most likely due

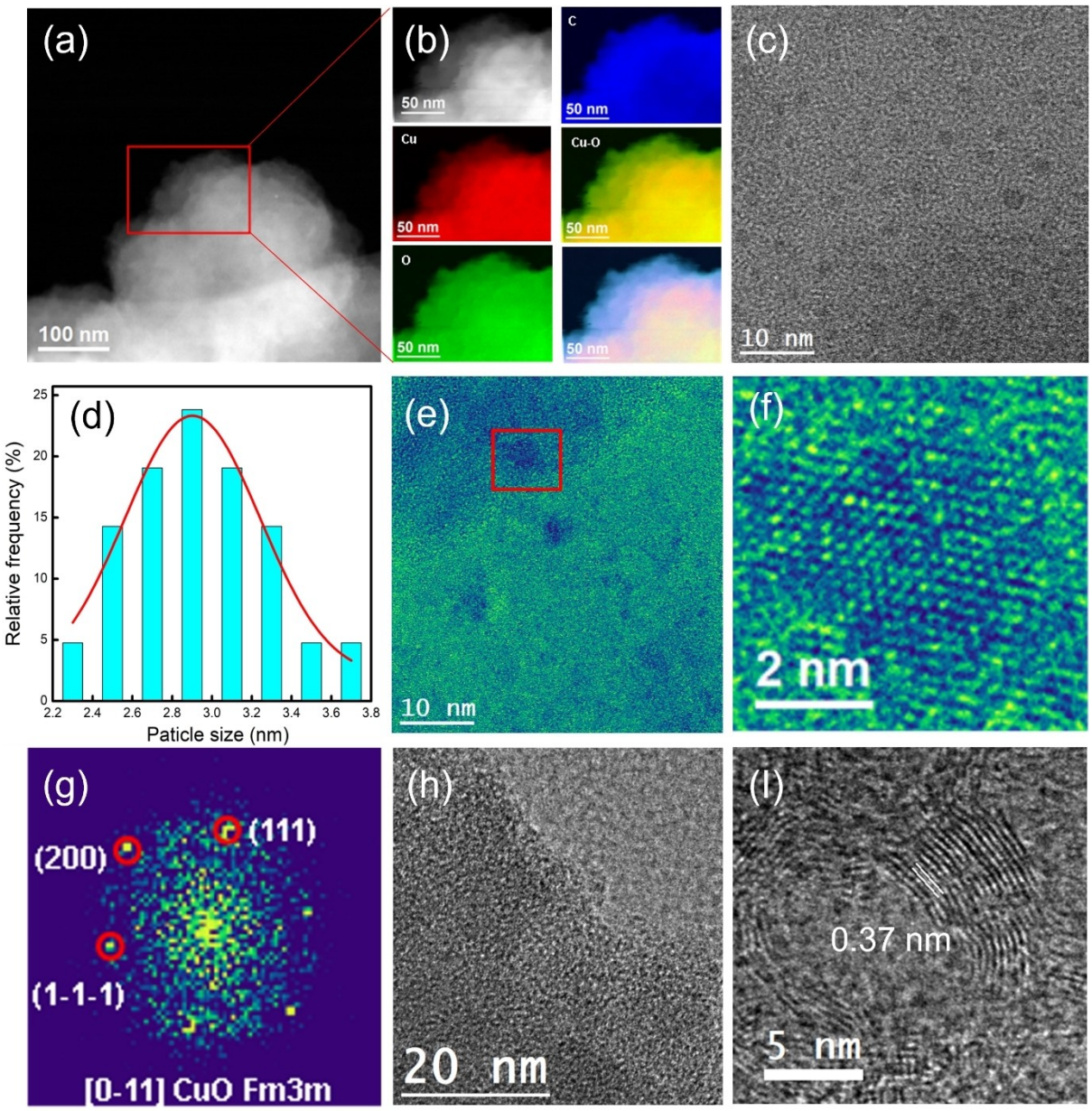

Figure 3. TEM Characterization of the as-prepared CuO/GDY and GDY. a) HAADF STEM image and b) the corresponding EELS mapping of the selected red-squared region of CuO/GDY; c) Bright-field TEM image and d) particle size distributions of CuO in GDY; e–g) HRTEM image of CuO in GDY, magnification of the red-squared region, and its corresponding indexed power spectrum (FFT); h) TEM image of pure GDY without CuO; i) HRTEM image of the interlayer spacing of pure GDY.

to the reduced accessibility to the active sites with the increased coverage of the TiO_2 surface. After removing CuO, the photocatalytic activity of GDY/TiO_2 decreased (Figure 5c), but remained much higher than those of CNT/TiO_2 and graphene/TiO_2, demonstrating the superiority of GDY for photocatalytic hydrogen evolution (Figure 5c). Photocurrent response experiments further confirmed that the synergetic effect between GDY and CuO as cocatalysts effectively promoted photogenerated carrier separation in TiO_2 (Figure S11). As a comparison, the noble metal platinum (Pt), a state-of-art cocatalyst for hydrogen evolution, was deposited on TiO_2 to prepare a series of Pt/TiO_2 photocatalysts. Remarkably, the performance of 5 % CuO/GDY/TiO_2 was better than that of 0.1 % Pt/TiO_2 and 0.2 % Pt/TiO_2 and even comparable to the 0.5 % Pt/TiO_2 (Figure 5d,e), indicating the potential industrial value of the CuO/GDY for photocatalysis. It is worth noting that the weight percent of CuO in 5 % CuO/GDY/TiO_2 was actually calculated to be 0.49 %, close to the weight percent of Pt in 0.5 % Pt/TiO_2. To illustrate the stability of the photocatalyst, recycling experiments were performed based on the most active 5 % CuO/GDY/TiO_2 sample. The CuO/GDY/TiO_2 sample maintained high activity even after four cycles under identical conditions, indicating excellent stability (Figure 5f).

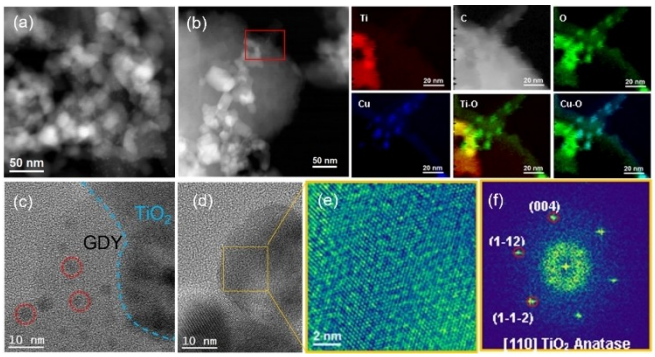

Figure 4. The characterization of CuO/GDY/TiO_2 composites. a) HAADF STEM image and b) HAADF STEM image and the corresponding EELS mapping of the selected red-squared region of CuO/GDY/TiO_2; c) HRTEM image of the interface of CuO, GDY and TiO_2 (the red circles: CuO NPs); d–f) HRTEM image of TiO_2, magnification of the yellow-squared region, and its corresponding indexed power spectrum (FFT).

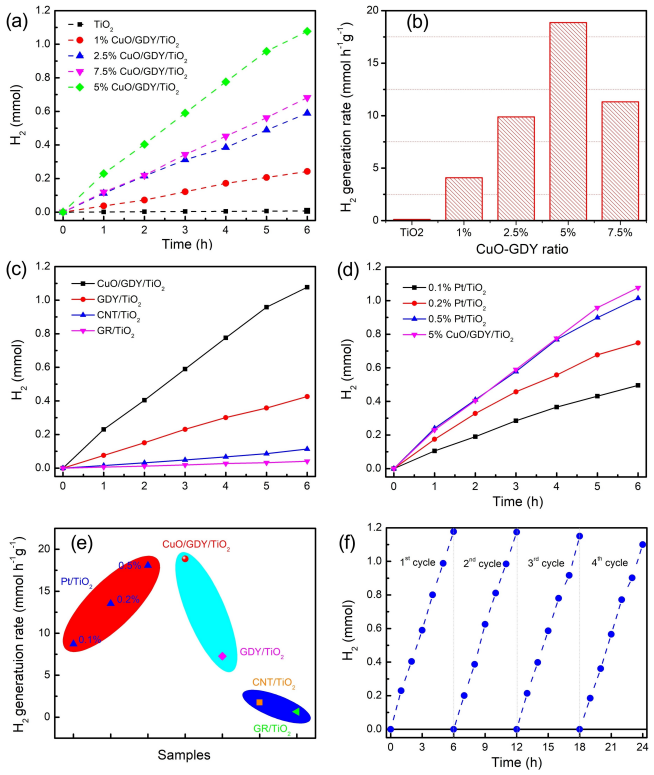

Figure 5. Photocatalysis performance test of the prepared samples. a) Hydrogen evolution of CuO/GDY/TiO_2 nanocomposites with different contents; b) H_2 generation rate based on the various CuO/GDY/TiO_2 nanocomposites; c) H_2 evolution of CuO/GDY/TiO_2, GDY/TiO_2, CNT/TiO_2 and GR/TiO_2; d) H_2 evolution of CuO/GDY/TiO_2 and TiO_2 with different Pt loading content; e) comparison of H_2 generation rate based on different photocatalysts; f) cycling measurement of hydrogen evolution of 5% CuO/GDY/TiO_2.

All these results demonstrate the great potential of the CuO/GDY powder as catalysts.

To better understand the photocatalytic process, the optical band structure of the as-prepared GDY powder was evaluated by Tauc plot and XPS valence spectra. The direct optical band gap of GDY powder was determined to be ≈1.47 eV (Figure S12), which is a little larger than the calculated one. The slight difference may be due to defects (created by oxygen) and interlayer interactions in the samples. The valence band (VB) edge of the GDY powder was further measured as ≈1.12 V vs normal hydrogen electrode (NHE) (Figure S13). Accordingly, the conduction band (CB) edge is calculated at −0.35 V vs NHE. For TiO_2, the main exposed surface (101) was considered for the electron transfer processes because this plane is nonpolar and displays excellent performance for photoreduction reactions.[24] The CB and VB edges of the surface (101) were −0.78 V and 2.92 V vs NHE, respectively. Under UV/Visible light excitation, electron/hole pairs are generated at the TiO_2 surface, where electrons are localized in the CB while holes remain at the VB. The photogenerated holes are more likely to be accumulated in the GDY while electrons can be transferred to the CB of GDY due to the suitable band alignment between TiO_2 and GDY. Then, electrons are collected by CuO NPs and experience multireductions during this process leading to the formation of Cu^0, which serves as an efficient reduction site for proton reduction.[25] The reduction of Cu^{II} to Cu^0 is further confirmed by XPS analysis of the photocatalyst after reaction (Figure S14). Thus, the synergetic effect between GDY and CuO as cocatalysts can effectively suppress the photoinduced carrier recombination and improve photocatalytic H_2 evolution (Figure S15).

Conclusion

By using HEB-TMS as monomers, we developed a deprotection-free method to prepare GDY powder. In the presence of CuCl in DMF solvent, the yield of GDY powder was as high as ≈100%. Moreover, CuO nanoparticles with an average diameter of ≈2.9 nm were in situ formed on the GDY surface after the coupling reaction. Pure GDY can be further obtained by removing the CuO NPs. To demonstrate the potential of the prepared CuO/GDY, CuO/GDY as cocatalysts was hybridized with TiO_2 for photocatalytic hydrogen evolution. Benefiting from the in situ formed solid junction between GDY and CuO, the CuO/GDY/TiO_2 sample displayed an excellent photocatalytic activity with an optimal H_2 generation rate of 18 mmol h^{-1} g^{-1}, comparable to the state-of-art Pt/TiO_2 photocatalyst. This work provides a straightforward deprotection-free approach for directly synthesizing GDY powder, paving the way for new applications of GDY in catalysis and other sustainable energy applications.

Acknowledgements

J.L. acknowledges funding from the European Union's Horizon 2020 research and innovation program under the Marie Sklodovska-Curie Grant Agreement No 101030637. J.L. acknowledges the public grant overseen by the French

National Research Agency (ANR) as part of the "Investissements d'Avenir" program (Labex NanoSaclay, reference: ANR-10-LABX-0035) for his post-doc position. M.N.G. acknowledges the public grant overseen by the French National Research Agency (ANR) as part of the ERANET-ACT3 call program and the Paris Ile-de-France Region (DIM RESPORE-2021-27) for financial support. L.Z and L.-Z.W. are grateful for financial support from the Strategic Priority Research Program of the Chinese Academy of Science (XDB17000000), Key Research Program of Frontier Science of the Chinese Academy of Sciences (QYZDY-SSW-JSC029). ICN2 acknowledges funding from Generalitat de Catalunya 2017 SGR 327. ICN2 was supported by the Severo Ochoa program from Spanish MINECO (Grant No. SEV-2017-0706) and was funded by CERCA Programme/ Generalitat de Catalunya.

Conflict of Interest

The authors declare no conflict of interest.

Data Availability Statement

The data that support the findings of this study are available from the corresponding author upon reasonable request.

Keywords: Copper Oxide/Graphdiyne · Deprotection-Free Synthesis · Graphdiyne · Photocatalysis · In Situ Formation

[1] a) C. Huang, Y. Li, N. Wang, Y. Xue, Z. Zuo, H. Liu, Y. Li, *Chem. Rev.* **2018**, *118*, 7744–7803; b) X. Gao, H. Liu, D. Wang, J. Zhang, *Chem. Soc. Rev.* **2019**, *48*, 908–936; c) Y. Fang, Y. Liu, L. Qi, Y. Xue, Y. Li, *Chem. Soc. Rev.* **2022**, *51*, 2681–2709; d) H. Yu, Y. Xue, Y. Li, *Adv. Mater.* **2019**, *31*, 1803101; e) J. Li, X. Gao, L. Zhu, M. N. Ghazzal, J. Zhang, C.-H. Tung, L.-Z. Wu, *Energy Environ. Sci.* **2020**, *13*, 1326–1346.

[2] a) H. Pan, H. Zhang, H. Wang, J. Li, Y. Sun, W. Lu, X. Wang, *Appl. Surf. Sci.* **2020**, *513*, 145694; b) M. Long, L. Tang, D. Wang, Y. Li, Z. Shuai, *ACS Nano* **2011**, *5*, 2593–2600; c) D. Ma, Z. Zeng, L. Liu, X. Huang, Y. Jia, *J. Phys. Chem. C* **2019**, *123*, 19066–19076.

[3] a) Y. Zhao, H. Tang, N. Yang, D. Wang, *Adv. Sci.* **2018**, *5*, 1800959; b) N. Wang, J. He, K. Wang, Y. Zhao, T. Jiu, C. Huang, Y. Li, *Adv. Mater.* **2019**, *31*, 1803202; c) Z. Zuo, D. Wang, J. Zhang, F. Lu, Y. Li, *Adv. Mater.* **2019**, *31*, 1803762; d) C. Li, X. Lu, Y. Han, S. Tang, Y. Ding, R. Liu, H. Bao, Y. Li, J. Luo, T. Lu, *Nano Res.* **2018**, *11*, 1714–1721.

[4] a) R. Sakamoto, N. Fukui, H. Maeda, R. Matsuoka, R. Toyoda, H. Nishihara, *Adv. Mater.* **2019**, *31*, 1804211; b) Z. Jia, Y. Li, Z. Zuo, H. Liu, C. Huang, Y. Li, *Acc. Chem. Res.* **2017**, *50*, 2470–2478; c) L. Hui, X. Zhang, Y. Xue, X. Chen, Y. Fang, C. Xing, Y. Liu, X. Zheng, Y. Du, C. Zhang, F. He, Y. Li, *J. Am. Chem. Soc.* **2022**, *144*, 1921–1928; d) Y. Liu, Y. Gao, F. He, Y. Xue, Y. Li, *CCS Chem.* **2022**, https://doi.org/10.31635/ccschem.022.202202005.

[5] a) J. Li, X. Gao, B. Liu, Q. Feng, X.-B. Li, M.-Y. Huang, Z. Liu, J. Zhang, C.-H. Tung, L.-Z. Wu, *J. Am. Chem. Soc.* **2016**, *138*, 3954–3957; b) Y. Xue, B. Huang, Y. Yi, Y. Guo, Z. Zuo, Y. Li, Z. Jia, H. Liu, Y. Li, *Nat. Commun.* **2018**, *9*, 1460; c) X. P. Yin, H. J. Wang, S. F. Tang, X. L. Lu, M. Shu, R. Si, T. B. Lu, *Angew. Chem. Int. Ed.* **2018**, *57*, 9382–9386; *Angew. Chem.* **2018**, *130*, 9526–9530; d) Y. Fang, Y. Xue, L. Hui, H. Yu, Y. Li, *Angew. Chem. Int. Ed.* **2021**, *60*, 3170; *Angew. Chem.* **2021**, *133*, 3207; e) Y. Liu, Y. Xue, L. Hui, H. Yu, Y. Fang, F. He, Y. Li, *Nano Energy* **2021**, *89*, 106333.

[6] a) J. Li, A. Slassi, X. Han, D. Cornil, M.-H. Ha-Thi, T. Pino, D. P. Debecker, C. Colbeau-Justin, J. Arbiol, J. Cornil, M. N. Ghazzal, *Adv. Funct. Mater.* **2021**, *31*, 2100994; b) Y. Fang, Y. Xue, Y. Li, H. Yu, L. Hui, Y. Liu, C. Xing, C. Zhang, D. Zhang, Z. Wang, X. Chen, Y. Gao, B. Huang, Y. Li, *Angew. Chem. Int. Ed.* **2020**, *59*, 13021–13027; *Angew. Chem.* **2020**, *132*, 13121–13127; c) F. Xu, K. Meng, B. Zhu, H. Liu, J. Xu, J. Yu, *Adv. Funct. Mater.* **2019**, *29*, 1904256; d) J. Li, X. Gao, X. Jiang, X.-B. Li, Z. Liu, J. Zhang, C.-H. Tung, L.-Z. Wu, *ACS Catal.* **2017**, *7*, 5209–5213; e) L. Hui, Y. Xue, H. Yu, Y. Liu, Y. Fang, C. Xing, B. Huang, Y. Li, *J. Am. Chem. Soc.* **2019**, *141*, 10677–10683.

[7] a) J. He, N. Wang, Z. Yang, X. Shen, K. Wang, C. Huang, Y. Yi, Z. Tu, Y. Li, *Energy Environ. Sci.* **2018**, *11*, 2893–2903; b) J. Wan, Z. Zuo, Z.-Z. Shen, W.-P. Chen, G.-X. Liu, X.-C. Hu, Y.-X. Song, S. Xin, Y.-G. Guo, R. Wen, Y. Li, L.-J. Wan, *J. Am. Chem. Soc.* **2022**, *144*, 9354–9362; c) N. Wang, X. Li, Z. Tu, F. Zhao, J. He, Z. Guan, C. Huang, Y. Yi, Y. Li, *Angew. Chem. Int. Ed.* **2018**, *57*, 3968–3973; *Angew. Chem.* **2018**, *130*, 4032–4037.

[8] J. Li, Y. Chen, J. Gao, Z. Zuo, Y. Li, H. Liu, Y. Li, *ACS Appl. Mater. Interfaces* **2019**, *11*, 2591–2598.

[9] a) W. Fan, S. Zhang, C. Xu, H. Si, Z. Xiong, Y. Zhao, K. Ma, Z. Zhang, Q. Liao, Z. Kang, Y. Zhang, *Adv. Funct. Mater.* **2021**, *31*, 2104633; b) Z. Jin, M. Yuan, H. Li, H. Yang, Q. Zhou, H. Liu, X. Lan, M. Liu, J. Wang, E. H. Sargent, Y. Li, *Adv. Funct. Mater.* **2016**, *26*, 5284–5289; c) J. Li, T. Jiu, S. Chen, L. Liu, Q. Yao, F. Bi, C. Zhao, Z. Wang, M. Zhao, G. Zhang, Y. Xue, F. Lu, Y. Li, *Nano Lett.* **2018**, *18*, 6941–6947.

[10] a) Y. Kong, J. Li, S. Zeng, C. Yin, L. Tong, J. Zhang, *Chem* **2020**, *6*, 1933–1951; b) C. Yin, J. Li, T. Li, Y. Yu, Y. Kong, P. Gao, H. Peng, L. Tong, J. Zhang, *Adv. Funct. Mater.* **2020**, *30*, 2001396.

[11] a) J. Li, X. Gao, Z. Li, J.-H. Wang, L. Zhu, C. Yin, Y. Wang, X.-B. Li, Z. Liu, J. Zhang, C.-H. Tung, L.-Z. Wu, *Adv. Funct. Mater.* **2019**, *29*, 1808079; b) J. Zhou, X. Gao, R. Liu, Z. Xie, J. Yang, S. Zhang, G. Zhang, H. Liu, Y. Li, J. Zhang, Z. Liu, *J. Am. Chem. Soc.* **2015**, *137*, 7596–7599; c) J.-J. Wang, H.-J. Wang, C. Zhang, Y.-N. Gong, Y.-L. Bai, T.-B. Lu, *2D Mater.* **2021**, *8*, 044008; d) W. Rong, H. Zou, W. Zang, S. Xi, S. Wei, B. Long, J. Hu, Y. Ji, L. Duan, *Angew. Chem. Int. Ed.* **2021**, *60*, 466; *Angew. Chem.* **2021**, *133*, 470.

[12] G. Li, Y. Li, H. Liu, Y. Guo, Y. Li, D. Zhu, *Chem. Commun.* **2010**, *46*, 3256–3258.

[13] X. Gao, J. Li, R. Du, J. Zhou, M.-Y. Huang, R. Liu, J. Li, Z. Xie, L.-Z. Wu, Z. Liu, J. Zhang, *Adv. Mater.* **2017**, *29*, 1605308.

[14] R. Matsuoka, R. Sakamoto, K. Hoshiko, S. Sasaki, H. Masunaga, K. Nagashio, H. Nishihara, *J. Am. Chem. Soc.* **2017**, *139*, 3145–3152.

[15] a) X. Gao, Y. Zhu, D. Yi, J. Zhou, S. Zhang, C. Yin, F. Ding, S. Zhang, X. Yi, J. Wang, L. Tong, Y. Han, Z. Liu, J. Zhang, *Sci. Adv.* **2018**, *4*, eaat6378; b) J. Zhou, Z. Xie, R. Liu, X. Gao, J. Li, Y. Xiong, L. Tong, J. Zhang, Z. Liu, *ACS Appl. Mater. Interfaces* **2019**, *11*, 2632–2637.

[16] a) Z. Zuo, H. Shang, Y. Chen, J. Li, H. Liu, Y. Li, Y. Li, *Chem. Commun.* **2017**, *53*, 8074–8077; b) H. Shang, Z. Zuo, H. Zheng, K. Li, Z. Tu, Y. Yi, H. Liu, Y. Li, Y. Li, *Nano Energy* **2018**, *44*, 144–154.

[17] R. Kulkarni, J. Huang, M. Trunk, D. Burmeister, P. Amsalem, J. Müller, A. Martin, N. Koch, D. Kass, M. J. Bojdys, *Chem. Sci.* **2021**, *12*, 12661–12666.

[18] a) X. Zhu, J. Xiong, Z. Wang, R. Chen, G. Cheng, Y. Wu, *Small Methods* **2022**, *6*, 2101001; b) Y. Xin, K. Yu, L. Zhang, Y. Yang, H. Yuan, H. Li, L. Wang, J. Zeng, *Adv. Mater.* **2021**, *33*, 2008145; c) T. Zhang, X. Han, H. Liu, M. Biset-Peiró, J. Li, X. Zhang, P. Y. Tang, B. Yang, L. R. Zheng, J. R. Morante, J. Arbiol, *Adv. Funct. Mater.* **2022**, *32*, 2111446.
[19] Z. Zuo, F. He, F. Wang, L. Li, Y. Li, *Adv. Mater.* **2020**, *32*, 2004379.
[20] a) K. Ikegashira, Y. Nishihara, K. Hirabayashi, A. Mori, T. Hiyama, *Chem. Commun.* **1997**, 1039–1040; b) Y. Nishihara, K. Ikegashira, F. Toriyama, A. Mori, T. Hiyama, *Bull. Chem. Soc. Jpn.* **2000**, *73*, 985–990; c) Y. Nishihara, K. Ikegashira, K. Hirabayashi, J.-I. Ando, A. Mori, T. Hiyama, *J. Org. Chem.* **2000**, *65*, 1780–1787.
[21] G. Luo, X. Qian, H. Liu, R. Qin, J. Zhou, L. Li, Z. Gao, E. Wang, W.-N. Mei, J. Lu, Y. Li, S. Nagase, *Phys. Rev. B* **2011**, *84*, 075439.
[22] M. C. Biesinger, *Surf. Interface Anal.* **2017**, *49*, 1325–1334.
[23] a) Q. Zheng, G. Luo, Q. Liu, R. Quhe, J. Zheng, K. Tang, Z. Gao, S. Nagase, J. Lu, *Nanoscale* **2012**, *4*, 3990–3996; b) X. Qian, H. Liu, C. Huang, S. Chen, L. Zhang, Y. Li, J. Wang, Y. Li, *Sci. Rep.* **2015**, *5*, 7756.
[24] a) W. Jiao, L. Wang, G. Liu, G. Q. Lu, H.-M. Cheng, *ACS Catal.* **2012**, *2*, 1854–1859; b) T. R. Gordon, M. Cargnello, T. Paik, F. Mangolini, R. T. Weber, P. Fornasiero, C. B. Murray, *J. Am. Chem. Soc.* **2012**, *134*, 6751–6761.
[25] a) J. M. Valero, S. Obregón, G. Colón, *ACS Catal.* **2014**, *4*, 3320–3329; b) J. Yu, J. Ran, *Energy Environ. Sci.* **2011**, *4*, 1364–1371; c) Q. Xu, M. Knezevic, A. Laachachi, S. Franger, C. Colbeau-Justin, M. N. Ghazzal, *ChemCatChem* **2022**, *14*, e202200102.

Manuscript received: July 13, 2022
Accepted manuscript online: August 19, 2022
Version of record online: September 7, 2022